Available online at www.sciencedirect.com
SCIENCE DIRECT®
Journal of Power Sources 147 (2005) 128–135
JOURNAL OF POWER SOURCES
www.elsevier.com/locate/jpowsour

Electrical conductivity enhancement in heterogeneously doped scandia-stabilized zirconia

Chakrapani Varanasi *, Chetan Juneja, Christina Chen, Binod Kumar

University of Dayton Research Institute, USA

Received 27 December 2004; accepted 16 January 2005
Available online 14 March 2005

Abstract

Composites of 6 mol% scandia-stabilized zirconia materials (6ScSZ) and nanosize Al_2O_3 powder (0–30 wt.%) were prepared and characterized for electrical conductivity by the ac impedance method at various temperatures ranging from 300 to 950 °C. All the composites characterized showed improved conductivity at higher temperatures compared to the undoped ScSZ. An average conductivity of 0.12 S cm^{-1} was measured at 850 °C for 6ScSZ + 30 wt.% Al_2O_3 composite samples, an increase in conductivity up to 20% compared to the undoped 6ScSZ specimen at this temperature. Microstructural evaluation using scanning electron microscopy revealed that the ScSZ grain size was relatively unchanged up to 10 wt.% of Al_2O_3 additions. However, the grain size was reduced in samples with higher (20 and 30 wt.%) additions of Al_2O_3. Small grain size, reduced quantity of the 6ScSZ material (only 70%), and improved conductivity makes these ScSZ + 30 wt.% Al_2O_3 composites very attractive as electrolyte materials in view of their collective mechanical and electrical properties and cost requirements. The observed increase in conductivity values with the additions of an insulating Al_2O_3 phase is explained in light of the space charge regions at the 6ScSZ–Al_2O_3 grain boundaries.

Keywords: Ionic conductivity; Solid oxide fuel cells; Electrolyte; ScSZ

1. Introduction

A superior alternative to the developed tubular solid oxide fuel cell (SOFC) is a planar design. The planar design yields an enhanced stack performance and much higher power density as compared to the tubular design. The high power density is critical to reduced costs, as the amount of required material per KW is minimized. Furthermore, the planar design can use low-cost fabrication methods such as screen-printing and tape casting. However, electrical conductivity, mechanical strength, thermal robustness, durable sealant, and fracture initiation during thermal cycling are some of the technical issues that limit development and commercialization of the planar design.

Scandia-stabilized zirconia (ScSZ) materials are known to exhibit higher conductivity as compared to the state-of-the-art yttria-stabilized zirconia (YSZ) materials. The conductivity enhancement in the ScSZ material is attributed to the minimal difference in ionic radii of the host Zr and dopant Sc [1]. The activation energy for the transport of oxygen ions in the ScSZ materials is also reduced as compared to the YSZ material [1]. There is a strong interest in the ScSZ materials, primarily motivated by improved conductivity, and a number of groups, specifically in Japan, are pursuing active research efforts [2–4].

A number of different approaches can be employed to enhance conductivity of the bulk electrolyte. The aforementioned YSZ and ScSZ materials were developed by the technique of homogeneous doping in which the host zirconium sites are replaced by yttrium and scandium sites. An alternate route to enhance bulk conductivity of stabilized zirconia is to employ a heterogeneous dopant. These heterogeneous dopants are insoluble in host YSZ or ScSZ and remain as a physically distinct phase of the bulk structure. For a number of ionic conductors, it has been demonstrated that the existence of an inert, heterogeneous

* Corresponding author. Tel.: +1 937 229 3527; fax: +1 937 229 3433.
E-mail address: pani.varanasi@udri.udayton.edu (C. Varanasi).

0378-7753/$ – see front matter © 2005 Elsevier B.V. All rights reserved.
doi:10.1016/j.jpowsour.2005.01.028

Table 1
Calculated and measured density of the 6ScSZ and Al_2O_3 composite samples

Sample	Al_2O_3 (wt.%)	Al_2O_3 (mol%)	Measured density ($g\,cm^{-3}$)	Theoretical density ($g\,cm^{-3}$)	Percent (%) of theoretical density
6SCSZ	0	0	5.82	5.87	99.15
6SCSZ + 10% Al_2O_3	10	11.91	5.36	5.68	94.37
6SCSZ + 20% Al_2O_3	20	23.3	5.205	5.49	94.81
6SCSZ + 30% Al_2O_3	30	34.26	5.03	5.31	94.73

dielectric phase in a conducting matrix can raise the ionic conductivity by orders of magnitude [5–11].

In a pioneering work, Liang [5] investigated polycrystalline lithium iodide doped with aluminum oxide and reported that lithium iodide doped with 35–45 mol% aluminum oxide exhibited conductivity on the order of $10^{-5}\,S\,cm^{-1}$ at 25 °C, about three orders of magnitude higher than that of the LiI conductivity. However, no significant amount of aluminum oxide was determined to be soluble in LiI; thus, the conductivity enhancement could not be explained by the classical doping mechanism and creation of Schottky defects such as in the LiI–CaF_2 system. Subsequently, a number of investigations have reported enhanced conductivity of silver in the AgI–Al_2O_3 system [6], copper in the CuCl–Al_2O_3 system [7], fluorine in the PbF_2–SiO_2 and PbF_2–Al_2O_3 systems [8], and lithium in polymer–ceramic composite electrolytes [9]. Four review papers [10–13] also document the developmental history and general characteristics of these fast ionic conductors. Analyses of these reviews point out that a new conduction mechanism evolves which augments the bulk conductivity of single-phase ionic conductors. The new conduction mechanism uses interfacial and/or space charge regions between the two primary components. The interfacial or space charge regions are formed because of the creation of charged vacancies and adsorption–desorption of ions. In effect, these regions are electrically active, which influences the transport of conducting ions.

Yamamoto et al. [14] found that the 8ScSZ (or12ScSZ) and Al_2O_3 composites show decrease in conductivity with increasing Al_2O_3 content. Badwal [15] also found a non-linear decrease in conductivity with increased insulator content but indicated that the conductor phase was continuous even up to 65% of the insulator phase. However, a recent investigation of heterogeneously doped YSZ materials with nanosize Al_2O_3 revealed that the Al_2O_3 dopant may lead to an enhancement and/or blockage of the conducting oxygen ions [16]. These effects are antagonistic and in effect may neutralize each other. The net result of Al_2O_3 doping in the aforementioned investigation [16] was small and conductivity variation revealed a minor influence on the total bulk conductivity. The objective of the present study was to further elucidate the composite effect in heterogeneously doped 6 mol% scandium-doped zirconium oxide (6ScSZ) materials. The composites may also provide improved fracture toughness, mechanical strength, and reduced cost. These attributes may lead to an electrolyte material that may satisfy requirements of the aforementioned planar design SOFC.

2. Experimental

ScSZ materials used were obtained from Tosoh Corporation[1] and the nanosize (∼24 nm) Al_2O_3 powder was obtained from Nanophase Technologies Corporation.[2] The amount of Scandia used in the ScSZ as per the manufacturer's specification is 6 mol% (6ScSZ). Appropriate amounts of 6ScSZ powder and Al_2O_3 powders were weighed and then mixed in a mortar and pestle to prepare 6ScSZ + Al_2O_3 composites containing 0, 10, 20, and 30 wt.% Al_2O_3. Powder batch compositions were pressed in a cold isostatic press at $3\,ton\,cm^{-2}$ pressure using collapsible tygon tubes to obtain specimens with dimensions of 10 mm diameter and approximately 2 cm long. The cylindrical shaped samples were heated at a rate of $20\,°C\,min^{-1}$ to 1520 °C in air and kept at this temperature for 4 h and then cooled at a rate of $20\,°C\,min^{-1}$ to 950 °C. Subsequently, they were soaked at 950 °C for 1 h before they were finally allowed to cool to room temperature by shutting the power off to the furnace. This procedure was followed to minimize the Al_2O_3 particle coarsening during heating which was an issue during an earlier investigation [16]. Several discs of 1 mm thickness were cut from these cylindrical specimens using a diamond saw.

The specimen density was determined using the Archimedes principle. One set of the discs were polished, thermally etched, and carbon coated by thermal evaporation for microstructural analysis using a Leica FE 960 scanning electron microscope (SEM). Similarly, polished specimens were also used for the hardness measurement using a Vickers hardness tester. Another set of discs was used to obtain X-ray diffraction (XRD) data using a Rigaku Rotaflex RV-200BH X-ray diffractometer operated at 40 kV, 150 mA current with a copper target.

AC impedance spectroscopy measurements in the 0.1–10^6 Hz frequency range were conducted on three different sets of discs of each composition using a Solatron 1260 impedance analyzer with 1287 electrochemical interface. The ac impedance data were obtained at several temperatures ranging from 300 to 950 °C. For the electrical conductivity measurements, the discs were coated on both sides with Pt paint and then fired in an ambient atmosphere furnace at 1000 °C for 1 h and subsequently furnace cooled. The

[1] Tosoh Corporation, 4560 Kaisei-Cho, Shinnanyo-shi, Yamaguchi-Ken 746-8501, Japan.
[2] Nanophase Technologies Corporation, 8205 S. Cass Avenue #105, Darien, IL 60561, USA.

fixture used in the present study consists of a machined glass-ceramic macor screw and socket design that can be tightened to provide intimate contact between the electrodes and the specimen. The fixture containing the specimen is inserted into a tube furnace and the data collected at several temperatures after stabilizing for 15 min at each temperature. The thermocouple was placed closest to the fixture in each measurement to ensure accuracy of the temperature measurement. A single crystal YSZ specimen was also characterized to establish the baseline for the ac impedance measurement. The same fixture and similar experimental procedure was used for the three sets of specimens to determine measurement errors and establish limits.

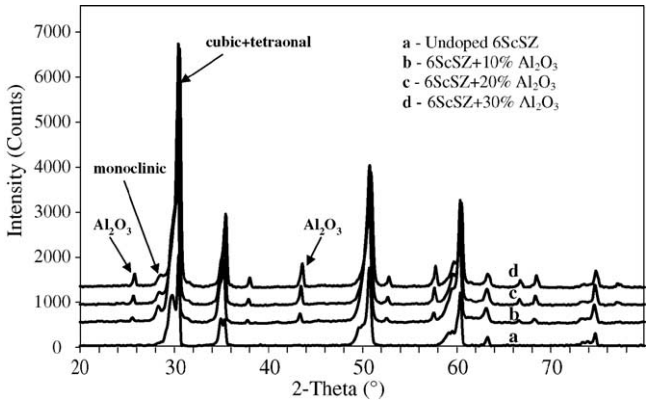

Fig. 1. XRD patterns taken from the sintered pellets of 6ScSZ + Al_2O_3 composites. (a) Un-doped 6ScSZ; (b) 6ScSZ + 10% Al_2O_3; (c) 6ScSZ + 20% Al_2O_3; and (d) 6ScSZ + 30% Al_2O_3.

3. Results and discussion

Table 1 presents calculated and measured densities of specimens doped with different concentrations of Al_2O_3. Since the density of Al_2O_3, 3.97 g cm^{-3}, is lower than the density of the stabilized zirconia, the densities of all doped specimens decrease with increasing concentration of the dopant. Also as expected, the measured densities are lower than the theoretical densities. However, with the increase of Al_2O_3 concentration, the difference between the measured

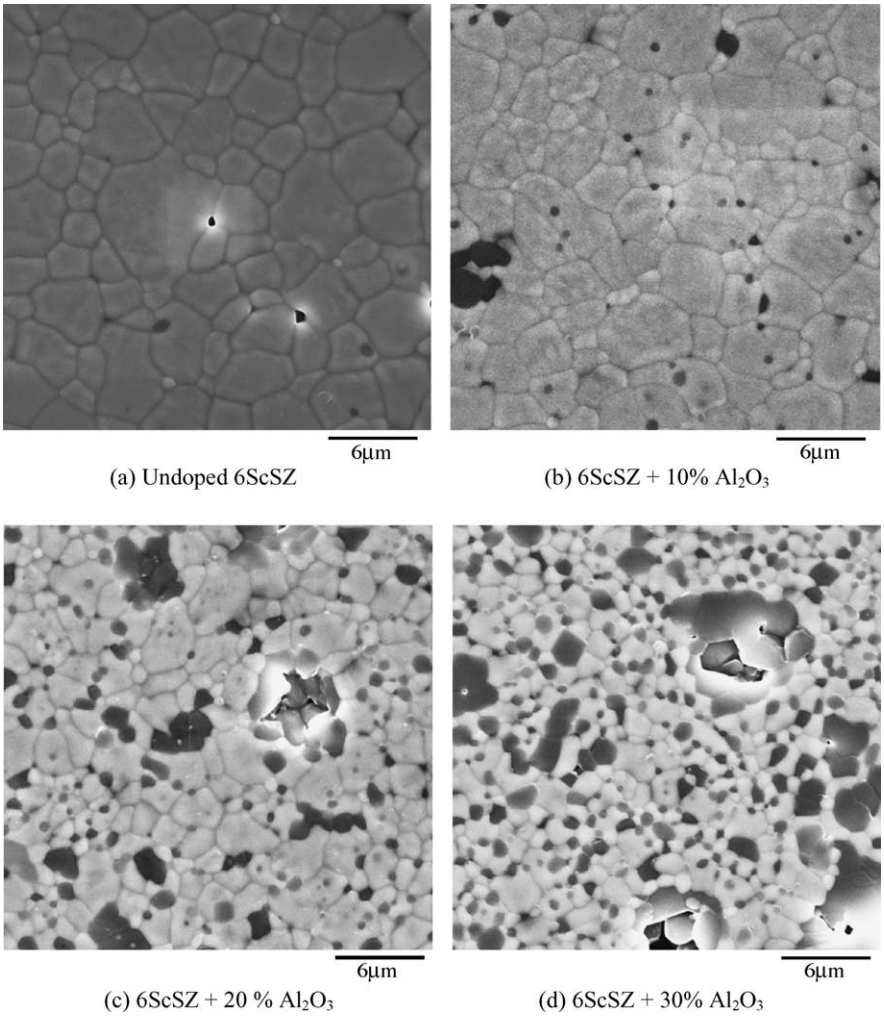

Fig. 2. Scanning electron micrographs of polished and etched 6ScSZ + Al_2O_3 composites. (a) Undoped 6ScSZ; (b) 6ScSZ + 10 wt.% Al_2O_3; (c) 6ScSZ + 20 wt.% Al_2O_3; and (d) 6ScSZ + 30 wt.% Al_2O_3. The dark contrast phase is Al_2O_3 and the light color phase is ScSZ.

density and the theoretical density increased. This observation is consistent with the earlier findings with YSZ–Al_2O_3 composites [16]. The Al_2O_3 particles inhibit the sintering and grain growth of the 6ScSZ grains and perhaps trap some porosity in the microstructure, thereby reducing the density. However, since the density greater than 94% of the theoretical values is achieved even with 30 wt.% of Al_2O_3, it was not considered to be a significant issue for further investigation.

As mentioned earlier, the fixture used in the present study requires the tightening of a macor screw to obtain good electrical contact, and so the samples are required to have good strength and undergo repeated measurements without developing cracks. The Vickers hardness obtained from the polished samples varied from 1337 to 1398 without a specific trend. It is interesting to note that no hardness degradation was measured even after 30% of 6ScSZ was replaced with Al_2O_3.

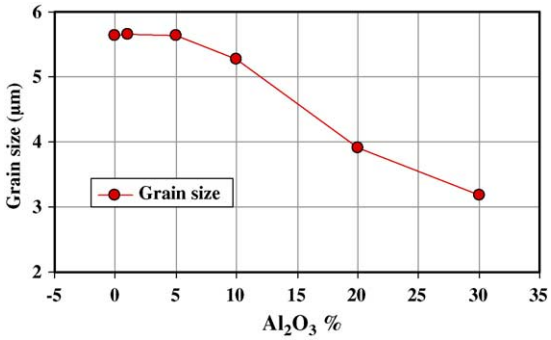

Fig. 3. ScSZ grain size variation with Al_2O_3 additions in the sintered pellets.

All the composite samples in this study exhibited high mechanical integrity so that repeated measurements on a single, thin (≅0.05 cm) specimen can be made without fracturing it.

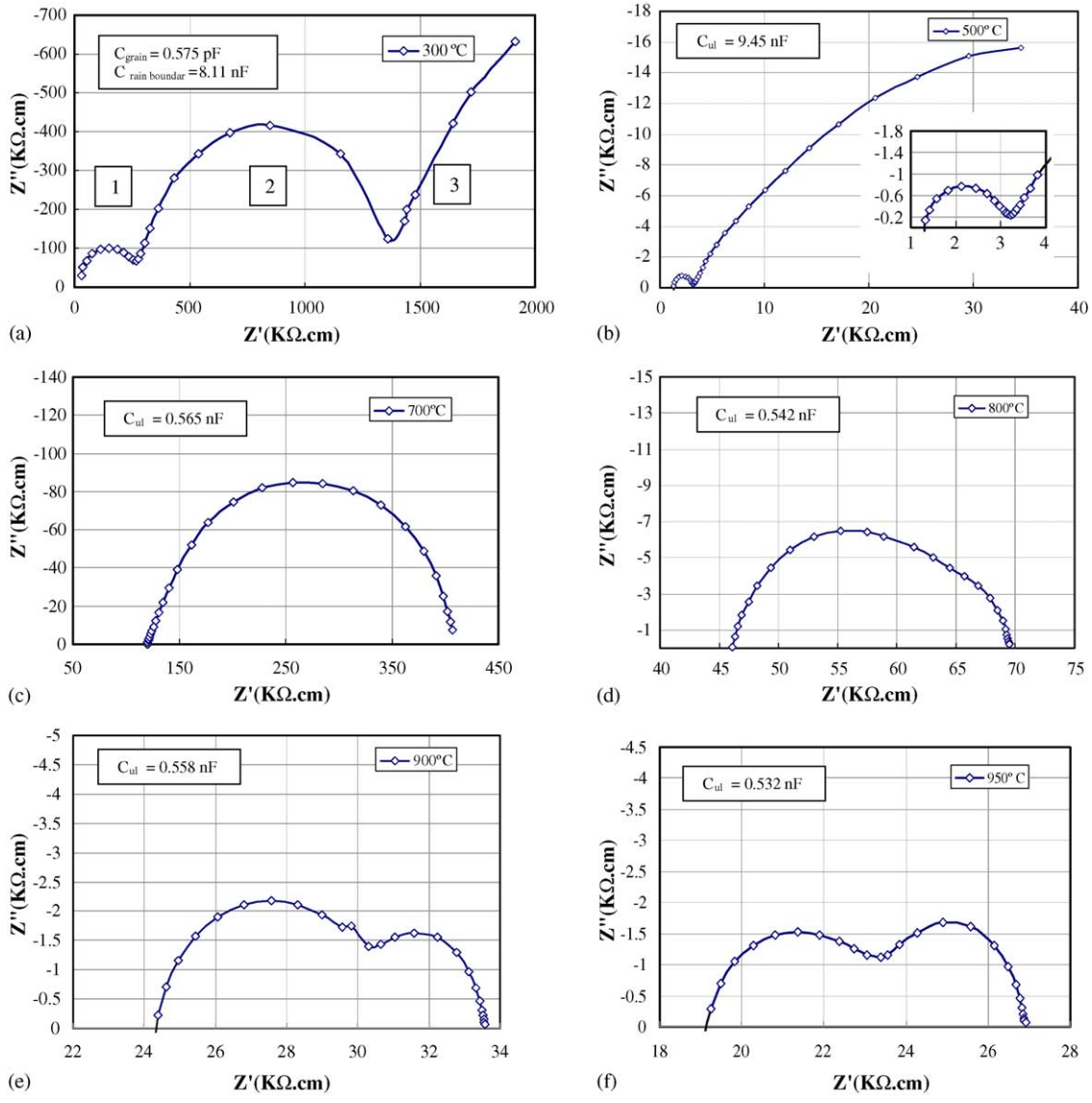

Fig. 4. Impedance plots of SSZ + 30% Al_2O_3 at different temperatures (a) 300 °C, (b) 500 °C, (c) 700 °C, (d) 800 °C, (e) 900 °C, and (f) 950 °C.

Fig. 1(a)–(d) shows the XRD patterns obtained from the sintered specimen. It is noted that in the undoped 6ScSZ specimen, both tetragonal and cubic phases are present, Fig. 1(a). The most intense XRD peak corresponding to these two phases is present at around $2\theta = 30^\circ$. The addition of nanosize Al_2O_3 leads to the formation of the monoclinic phase shown by an arrow in the diffraction pattern of the composite containing 30 wt.% Al_2O_3, Fig. 1(d). The observations relating to the existence of crystalline phases in the undoped specimen, i.e., presence of both tetragonal and cubic phases, are consistent with earlier reports [1,3].

The phase diagram in the ZrO_2–Sc_2O_3 system [17] predicts the existence of a monoclinic phase if the specimen is cooled under equilibrium conditions. However, the undoped ScSZ specimen processed under similar conditions does not show the presence of the monoclinic phase. Therefore, the

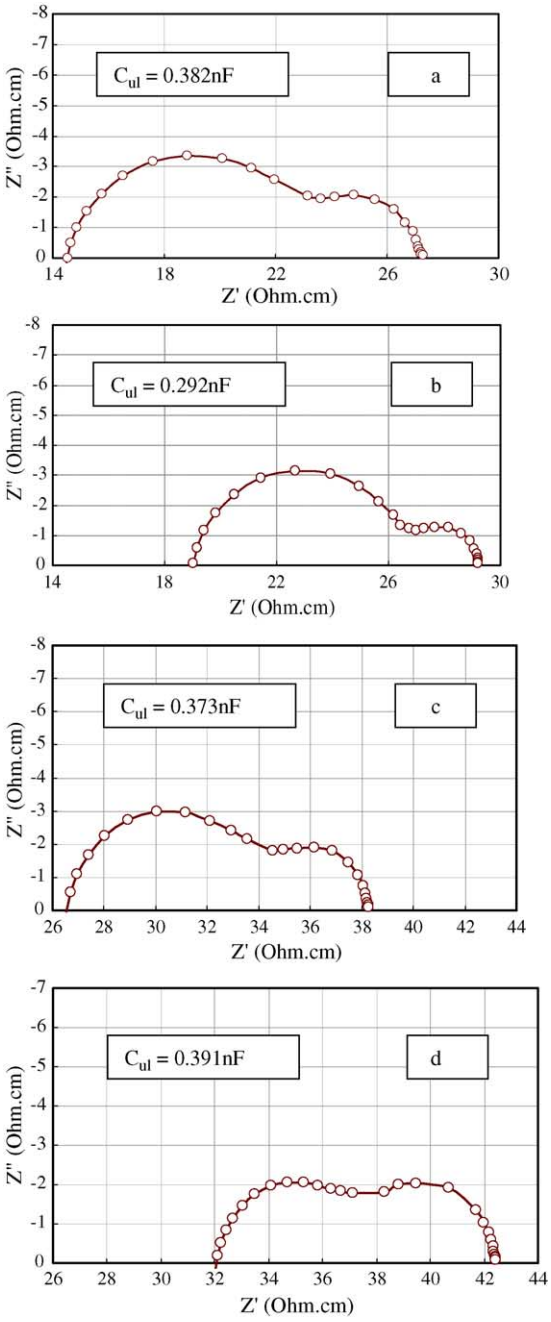

Fig. 5. Impedance plots of (a) undoped 6ScSZ; (b) 6ScSZ + 10% Al_2O_3; (c) 6ScSZ + 20% Al_2O_3; (d) 6ScSZ + 30% Al_2O_3 at 850 °C.

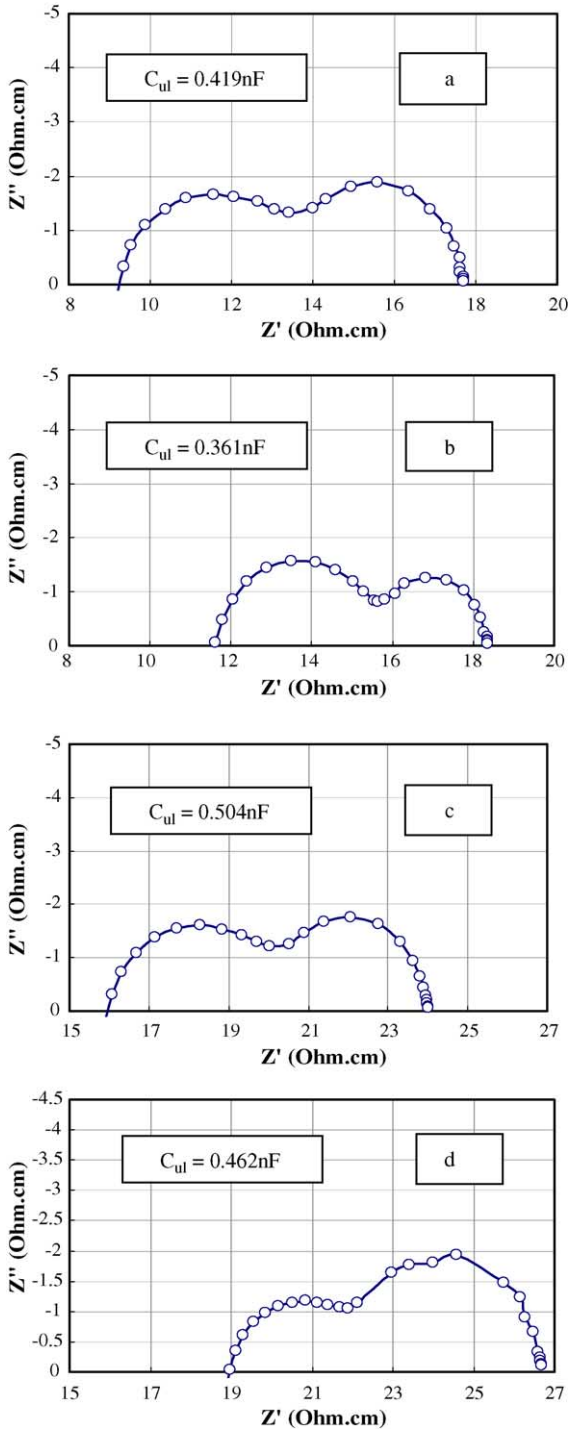

Fig. 6. Impedance plots of (a) undoped 6ScSZ; (b) 6ScSZ + 10% Al_2O_3; (c) 6ScSZ + 20% Al_2O_3; (d) 6ScSZ + 30% Al_2O_3 at 950 °C.

existence of the monoclinic phase in the Al_2O_3 doped specimens must be related to the presence of Al_2O_3 and perhaps the existence of a ScSZ–Al_2O_3 solid solution. The ionic radii of Zr^{4+}, Sc^{4+}, and Al^{+} are 0.80, 0.81, and 0.50 Å and considering the large difference in the ionic radii of Zr^{4+}/Sc^{4+} and Al^{3+} sites, only a very limited solid solubility of Al_2O_3 in the ScSZ can be expected.

With the increased additions, the intensity of peaks corresponding to Al_2O_3 phase is increased and no additional extraneous peaks were observed indicating that no chemical interactions with the matrix have taken place. Also, no noticeable peak shift was observed which indicates that the solubility of Al_2O_3 in ScSZ is minimal due to a large difference in the ionic radii. As noted earlier, up to 1 wt.% Al_2O_3 can dissolve in YSZ when maintained at 1500 °C for 24 h [18]. Since in the present study the specimens were kept at 1500 °C for a short period (only 4 h), the solubility is expected to be lower.

Fig. 2 shows the scanning electron micrographs of the specimens doped with different concentrations of Al_2O_3. A microstructure with some porosity can be observed in all the samples. While some of the Al_2O_3 particles (dark areas) can be observed at the grain boundaries in the composite samples, occasionally some particles were also entrapped inside the ScSZ grains. A reduction in grain size by a factor of 2 is observed in 6ScSZ with 30 wt.% Al_2O_3 composites as compared to undoped 6ScSZ samples. The variation in ScSZ grain size with the Al_2O_3 additions is shown in Fig. 3. Although nanosize Al_2O_3 was used, a wide size distribution of Al_2O_3 particles is observed in 6ScSZ with 20 and 30 wt.% Al_2O_3 composite specimens, Fig. 2(c) and (d). The average grain size of Al_2O_3 is about 1 μm in these specimens [2 (c) and (d) micrographs]. In higher concentrations of Al_2O_3 doped samples (20 and 30% doping level), the coarsening of the particles is evident at the triple points. Dissolution and re-precipitation of Al_2O_3, including particle coarsening is attributed to the observed microstructures. The ScSZ grain growth was inhibited at higher Al_2O_3 doping levels, resulting in small grain size. It may also be possible to modify the heat treatments to obtain fine grain size of Al_2O_3 in these composites.

AC impedance plots of one 6ScSZ +30 wt.% Al_2O_3 specimen obtained at several temperatures (300–950 °C) are shown in Fig. 4(a)–(f). It can be seen that the appearance shown by the semicircles and their intersections with real axis (Z') change with the temperature of the measurement. The intercept of the first semicircle closest to the origin in all the plots is due to the contact resistance arising at the electrolyte–electrode interface. There are three different regions in the 300 °C temperature measurement plot. The first semicircle (marked 1) in Fig. 4(a) from the left is due to the grain resistance, the second semicircle (marked 2) results from the grain boundary resistance and the third incomplete semicircle (marked 3) is due to the resistive capacitive component of the electrode-electrolyte interface. However, as the temperature of the measurement is increased, the capacitances of the grain boundary and grain become comparable and one of the semicircles (corresponding to the grain) disappears. Hence, at high temperatures, the first semicircle is due to the combined grain and grain boundary i.e., bulk electrical properties (resistance and capacitance) and the second semicircle is due to the electrode–electrolyte interface. This interpretation of the impedance spectra was used for all the data collected in this study.

Fig. 5(a)–(d) shows the complex impedance plots obtained from the samples with different amounts of Al_2O_3 additions at 850 °C. It can be seen that all the curves show two semicircles and the diameter of the first semicircle corresponds to the bulk resistance including grain and grain boundary is reduced with increasing amounts of Al_2O_3, indicating that the bulk conductivity has increased. The second semicircle diameter that depicts electrical properties of the electrode-electrolyte interface varies from specimen to specimen in an inconsistent manner. The resistance and capacitance values shown in the figures were obtained by fitting the spectra with the program Z view™ (version 2.3 d, Scribner Associates Inc.). Fig. 6(a–d) again shows the impedance plots of specimens containing various amounts of Al_2O_3 at 950 °C. The trend is very similar to Fig. 5(a–d), in that the diameter of the first semicircle decreases with temperature and the second semicircle, showing an inconsistent trend. The bulk resistivity of the specimen which is equivalent to the diameter of the first semicircle and obtained directly from Figs. 5 and 6 are plotted in Fig. 7 to show the trend of resistivity reduction variation with the composition. It can be seen that at these temperatures, the resistance of the electrolytes is reduced by approximately 25% as Al_2O_3 concentration is increased.

Fig. 8(a–d) shows the mean conductivity of the samples measured at 800, 850, 900, and 950 °C as a function of Al_2O_3 concentration. Three specimens were characterized at each Al_2O_3 concentration. The conductivity values determined from these measurements, their mean and a solid line obtained by a regression analysis are also shown in Fig. 8. It is noted that at all temperatures ranging from 800 to 950 °C the conductivity improves with the addition of Al_2O_3. The spread in the measured conductivity values appears to increase with increasing concentration of Al_2O_3. This is expected because

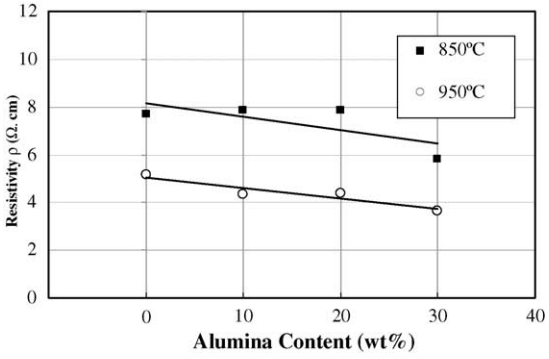

Fig. 7. The diameter of the first circle in Figs. 5 and 6 that represent the resistivity of the electrolyte is plotted as a function of the Al_2O_3 content.

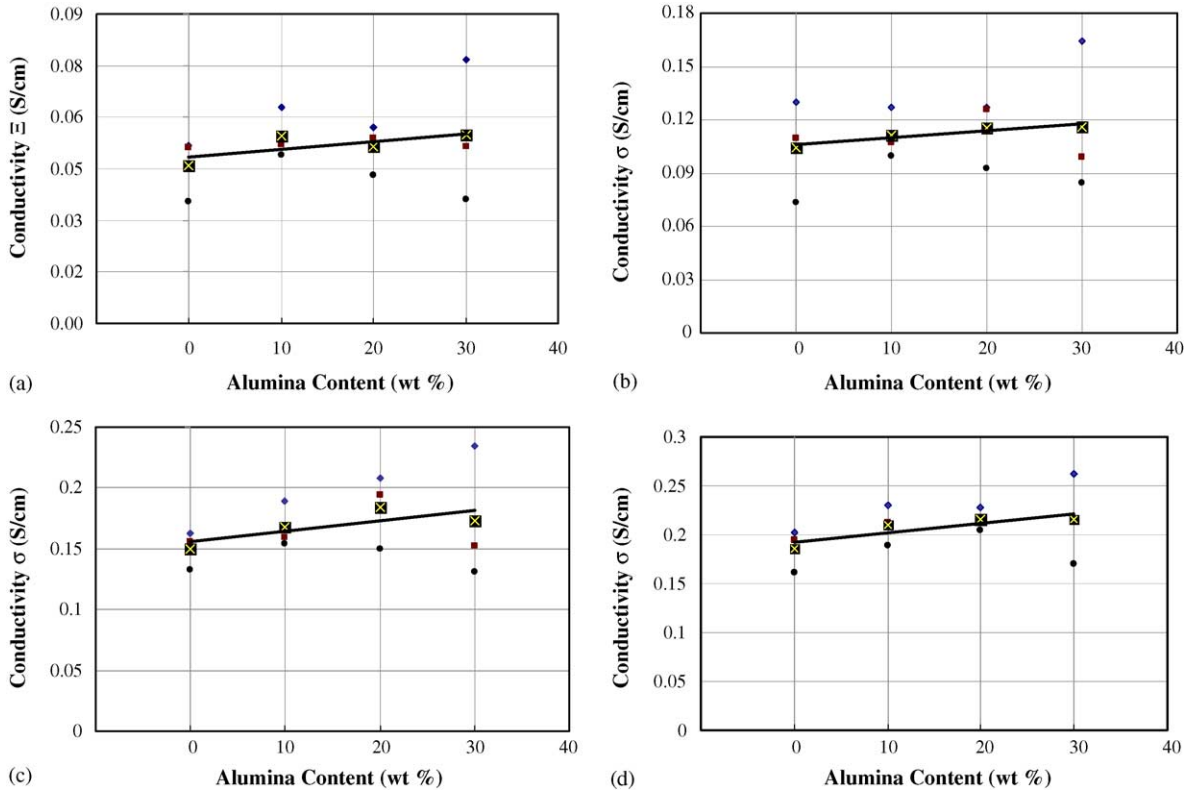

Fig. 8. The mean conductivity (as designated by the symbol ×) of the samples measured at various temperatures: (a) 800 °C, (b) 850 °C, (c) 900 °C, and (d) 950 °C without correcting for the non-conducting Al_2O_3 phase.

statistical distribution of the percolation path through which oxygen ions can be transported increases with higher Al_2O_3 concentration.

Fig. 9 presents normalized conductivity; i.e., conductivity of the composite specimen divided by the volume of the active material (6ScSZ). The conductivities at 900 °C show greater enhancements as compared to 800 °C as Al_2O_3 was increased. If the blocking effect of Al_2O_3 is taken into account, the conductivity data should exhibit a rapid drop with Al_2O_3 content. The conductivity enhancement as noted in Fig. 9 must therefore, be attributed to the formation of space charge regions which provide local electric fields and accelerates the transport of oxygen ions, thereby increasing the conductivity. The space charge mechanism assisted transport of conducting ions has been reported earlier [16].

Fig. 10 shows Arrhenius plots of the conductivity of specimens in the 800–950 °C temperature range. The activation energy for the transport of oxygen ions was determined to be

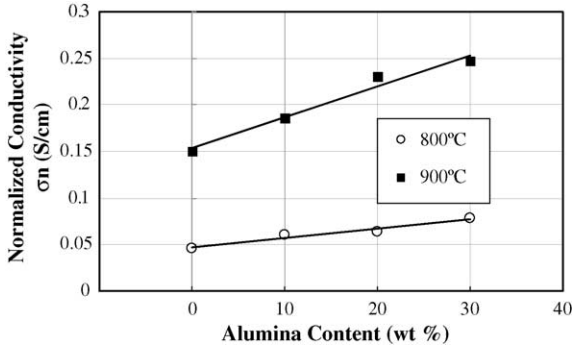

Fig. 9. The average conductivity of the samples measured at 800 and 900 °C after correcting for the non-conducting Al_2O_3 phase.

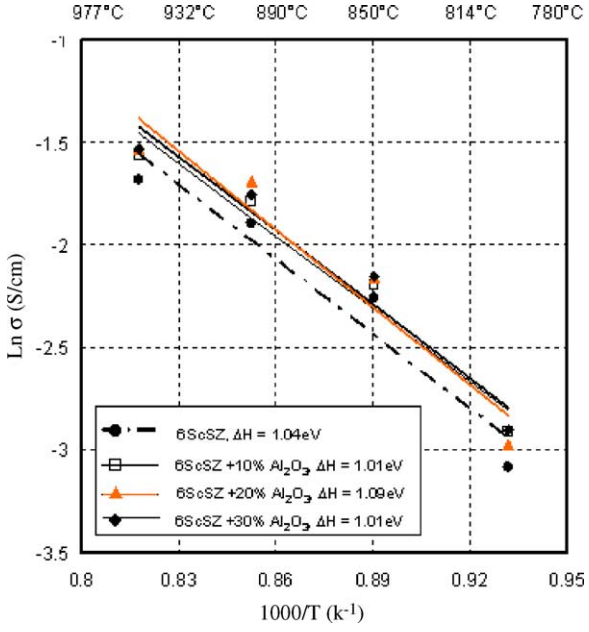

Fig. 10. Arrhenius plots of all the 6ScSZ + Al_2O_3 composites.

in the range of 1.01–1.09 eV which is consistent with values reported in the literature. It is apparent that the conduction mechanism in these composites remains essentially the same.

4. Summary and conclusions

This paper investigated the effects of nanosize Al_2O_3 doping on the conductivity of 6 mol% scandia stabilized zirconia. The Al_2O_3 doping concentration was varied from 0 to 30 wt.% and the specimens were characterized by SEM, XRD, and impedance spectroscopy. The significant conclusions of the investigation are summarized as follows:

1. The composite specimens of this investigation were truly heterogeneous as evidenced by SEM micrographs and XRD data. The solid solubility between the ScSZ and Al_2O_3 was minimal, as no significant change in the *d*-spacings occurred.
2. Initially, the grain size remained unaffected with the addition of Al_2O_3 up to about 5 wt.%. With further addition of Al_2O_3, the grain size decreased to about 3 μm for 30 wt.% Al_2O_3.
3. The conductivity data of the bulk specimen obtained from the ac measurement revealed enhancement of the total, bulk conductivity in the 800–950 °C temperature range due to the addition of Al_2O_3. The conductivity increased as the Al_2O_3 content was increased up to 30 wt.%. Both grain and grain boundary conductivities were characterized and at these temperatures contributions from these merge into a single semicircle in the impedance plot.
4. The conductivity variation was explained on the basis of antagonistic influences of Al_2O_3 doping. The doping leads to the creation of space charge regions in the vicinity of ScSZ-Al_2O_3 boundaries, which should enhance transport of oxygen ions and thus conductivity. The presence of Al_2O_3 may also lead to a blocking effect, which suppresses conductivity. The net result of the two antagonist influences is small but positive and reflected by an enhancement in conductivity as the concentration of Al_2O_3 was increased.
5. The activation energy for the transport of conducting oxygen ion was calculated to be around 1 eV and was found to be similar for undoped and doped specimens.

Acknowledgment

The authors gratefully acknowledge the financial support by the Air Force Research Laboratory, Propulsion Directorate, under Contract No. F33615-02-D-2299.

References

[1] O. Yamamoto, Y. Arati, Y. Takeda, N. Imanishi, Y. Mizutani, M. Kawai, Y. Nakamura, Solid State Ionics 79 (1995) 137.
[2] Y. Arachi, H. Sakai, O. Yamamoto, Y. Takeda, N. Imanishai, Solid State Ionics 121 (1999) 133.
[3] M. Hirano, S. Watanabe, E. Kato, Y. Mizutani, M. Kawai, Y. Nakamura, Solid State Ionics 111 (1998) 161.
[4] Y. Mizutani, M. Tamura, M. Kawai, Solid State Ionics 72 (1994) 271.
[5] C.C. Liang, J. Electrochem. Soc. 120 (1973) 1289.
[6] K. Shahi, J.B. Wagner, Solid State Ionics 3/4 (1981) 295.
[7] T. Jow, J.B. Wagner, J. Electrochem. Soc. 126 (1979) 1963.
[8] K. Hariharan, J. Maier, J. Electrochem. Soc. 142 (10) (1995) 3469.
[9] B. Kumar, S.J. Rodrigues, L.G. Scanlon, J. Electrochem. Soc. 148 (10) (2001) 1191.
[10] R.C. Agrawal, R.K. Gupta, J. Mater. Sci. 34 (1999) 1131.
[11] A. Mikrajuddin, G. Shi, K. Okuyama, J. Electrochem. Soc. 147 (8) (2000) 3157–3165.
[12] P. Knauth, J. Electroceram. 5 (2) (2000) 111–125.
[13] B. Kumar, L.G. Scanlon, J. Power Sources 52 (1994) 261.
[14] O. Yamamoto, T. Kawahara, Y. Takeda, N. Imanishi, Y. Sakaki, Science and Technology of Zirconia V, Technomic, USA, 1993, pp. 733–741.
[15] S.P.S. Badwal, J. Mater. Sci. 18 (1983) 3230–3242.
[16] B. Kumar, C. Chen, C. Varanasi, J.P. Fellner, J. Power Sources 140 (2005) 12–20.
[17] F.M. Spiridonov, L.N. Popova, R.Ya. Popilskii, J. Solid State Chem. 2 (1970) 430.
[18] A.J. Feighery, J.T.S. Irvine, Solid State Ionics 121 (1999) 209–216.